Flagship Article

Nano Research
2022, 15(2): 758–764

ISSN 1998-0124 CN 11-5974/O4
https://doi.org/10.1007/s12274-021-3602-x

Fully rubbery synaptic transistors made out of all-organic materials for elastic neurological electronic skin

Hyunseok Shim[1], Seonmin Jang[1], Jae Gyu Jang[2], Zhoulyu Rao[1], Jong-In Hong[2], Kyoseung Sim[3], and Cunjiang Yu[1,4,5,6,7] (✉)

[1] *Materials Science and Engineering Program, University of Houston, Houston, TX 77204 USA*
[2] *Department of Chemistry, Seoul National University, Seoul 08826, Republic of Korea*
[3] *Department of Chemistry, Ulsan National Institute of Science and Technology (UNIST), Ulsan 44919, Republic of Korea*
[4] *Department of Mechanical Engineering, University of Houston, Houston, TX 77204 USA*
[5] *Department of Biomedical Engineering, University of Houston, Houston, TX 77204, USA*
[6] *Department of Electrical and Computer Engineering, University of Houston, Houston, TX 77204 USA*
[7] *Texas Center for Superconductivity, University of Houston, Houston, TX 77204, USA*

Received: 15 April 2021 / **Revised:** 13 May 2021 / **Accepted:** 18 May 2021

ABSTRACT

Neurologic function implemented soft organic electronic skin holds promise for wide range of applications, such as skin prosthetics, neurorobot, bioelectronics, human-robotic interaction (HRI), etc. Here, we report the development of a fully rubbery synaptic transistor which consists of all-organic materials, which shows unique synaptic characteristics existing in biological synapses. These synaptic characteristics retained even under mechanical stretch by 30%. We further developed a neurological electronic skin in a fully rubbery format based on two mechanoreceptors (for synaptic potentiation or depression) of pressure-sensitive rubber and an all-organic synaptic transistor. By converting tactile signals into Morse Code, potentiation and depression of excitatory postsynaptic current (EPSC) signals allow the neurological electronic skin on a human forearm to communicate with a robotic hand. The collective studies on the materials, devices, and their characteristics revealed the fundamental aspects and applicability of the all-organic synaptic transistor and the neurological electronic skin.

KEYWORDS

synaptic transistor, stretchable, electronic skin, all-organic

1 Introduction

Human and animal skins have built-in synapses to render closed-loop sense-actuation operations [1, 2]. Synapses are unique biological structures, which enable signal communication between neurons in biological nervous systems and are responsible for encoding sensations, thoughts, etc. [3–5]. With the fast advancement on material development, mechanical designs and device technologies, drastic advances on soft artificial skins have been made in the past decades [6–9]. In particular, neurologic function implemented artificial skin is very promising for a wide range of vital yet technically critical applications, such as neuroprosthetics, neurorobots, bioelectronic interfaces, human-robotic interaction (HRI), etc. [3, 10–16]. To implement the artificial skin with capabilities emulating those of the biological skin, in particular the synaptic functions, soft synaptic devices must be accomplished with similar mechanical softness and stretchability and can be seamlessly integrated with the skin devices.

To date, although some progress on integrating neurologic functions into artificial skins have been made, the progress is still nascent [17]. In addition, although there have been reports on deformable synaptic transistors [3, 10, 18], a stretchable synaptic transistor made out of all-organic materials has never been achieved before, which would possess the advantages of low cost [19], easy processibility [20], biocompatibility [21, 22] and deformability [23, 24].

Here, we report a fully rubbery synaptic transistor made out of all-organic materials and its neurologically integrated electronic skin in a fully rubbery format. Specifically, we developed the fully rubbery synaptic transistor using the rubbery semiconductor as a composite of poly(3-hexylthiophene) (P3HT) nanofibrils percolated in polydimethylsiloxane (P3HT-NFs/PDMS), the rubbery conductor as poly(3,4-ethylenedioxythiophene): polystyrene sulfonate (PEDOT:PSS) mixed with a nonvolatile surfactant plasticizer (Triton X-100), and the elastic gate dielectric as ion-gel. The all-organic synaptic transistor is achieved based on simple facile fabrication methods for different layer of materials. The characteristics of the devices are studied while they are under different levels of mechanical strains both along and perpendicular to the channel length directions. The synaptic transistor shows unique functions, existing in biological synapses, including excitatory postsynaptic current (EPSC), paired-pulse facilitation (PPF), and memory characteristics. Upon stretching by 30%, these characteristics were still maintained. In addition, we developed a neurological electronic skin in a fully rubbery format based on two mechanoreceptors (for synaptic potentiation or depression), each consisting of pressure-sensitive rubber

Address correspondence to cyu15@uh.edu

and a fully rubbery synaptic transistor. Each mechanoreceptor for synaptic potentiation and depression responds to physical touches by generating presynaptic pulses, which excite the synaptic transistor to render postsynaptic potentials. By converting tactile signals into Morse Code, potentiation and depression of EPSC signals allows the neurological electronic skin on a human forearm to communicate with a robotic hand. The collective studies on the materials, devices, and their characteristics demonstrated the fundamental aspects and applicability of the all-organic synaptic transistor and the neurological function implemented artificial skin.

2 Experimental

2.1 Preparation of P3HT-NFs/PDMS semiconductor

The P3HT-NFs solution was prepared by dissolving P3HT (2 mg) in dichloromethane (1 mL) at 80 °C, followed by cooling down at –20 °C. The solution was blended with a PDMS solution that was prepared by mixing the PDMS precursor (weight ratio of prepolymer: curing agent is 10:1) and dichloromethane (80 mg/mL) to obtain the P3HT-NFs/PDMS at the weight ratio of 1:4. The P3HT-NFs/PDMS solution was spin-coated at 2,000 rpm for 60 s, followed by thermal annealing at 90 °C for 10 min to form the P3HT-NFs/PDMS thin film.

2.2 Preparation of ion gel dielectric

The solution was prepared by mixing poly(vinylidene fluoride-co-hexafluoropropylene) (PVDF-HFP), 1-ethyl-3-methylimidazolium bis(trifluoromethylsulfonyl)imide (EMIM-TFSI), and acetone in a weight ratio of 1:4:7 at 80 °C for 8 hours. The ion gel film was achieved by curing in the vacuum oven at 70 °C for 12 hours after pouring the solution on a precleaned glass substrate. The solidified ion gel can be easily cut into desired shapes to laminate on P3HT-NFs/PDMS film.

2.3 Preparation of surface modified elastomeric substrate

The PDMS precursor was prepared by mixing the prepolymer and curing agent in a weight ratio of 10:1 and spin-coating on the glass substrate at 300 rpm for 30 s, followed by curing in oven at 90 °C for 2 hours. For the hydrophilic surface modification of PDMS, the prepared PDMS film was treated with UV-O_3 for 20 min and immersed in APTES solution (3 wt.% in deionized (DI) water) for 20 min.

2.4 Preparation of stretchable nanostructured PEDOT:PSS conductor

Aqueous PEDOT:PSS solution (Clevios™ PH1000, Heraeus) mixed with 3 wt.% of surfactant (Triton X-100, Aldrich) was stirred for 12 hours. The PEDOT:PSS film was patterned on a glass substrate by spin coating the mixture solution through a Kapton film-based shadow mask. After removing the shadow mask, a surface modified PDMS substrate was pressed onto the patterned PEDOT:PSS film on the glass substrate and peeled off. The resulted film was annealed on a hot plate at 140 °C for 10 min to enhance its electrical conductivity.

2.5 Material characterization and device measurements

The surface morphology of the composite semiconductor and conductor was characterized using atomic force microscopy (AFM, Bruker) under the tapping mode. Electrical properties of the synaptic transistor were characterized by a probe station (H100, Signatone) equipped with a semiconductor characterization system (4200-SCS, Keithley Instruments Inc). A function generator (DG4062, RIGOL Technologies Inc) was used to apply the presynaptic voltage on the gate electrode. The postsynaptic current was measured by applying a constant V_{ds} between the source and the drain.

3 Results

Figure 1(a) shows the schematic illustration of the fully rubbery synaptic transistor implemented artificial skin, i.e., neurological electronic skin, in an exploded view. The neurological electronic skin consists of three layers: two patterned electrodes (bottom) and pressure-sensitive rubber (middle) connected to the gate electrode of a fully rubbery synaptic transistor (top). The pressure-sensitive rubber is used for mimicking rubbery mechanoreceptor. The PDMS encapsulation on conductive rubber is conducted for insulation between our hand and electrode. Most importantly, the deformable synaptic transistor, a core component in the skin, consists of all-organic materials, including the semiconductor, conductor, dielectric, and substrate, as shown in Fig. 1(b). Both the semiconducting and conductive films, which were obtained through nanostructure engineering, under 0% and 30% strain are presented in Fig. 1(c). Since all the materials are in a rubbery format, the neurological electronic skin can be stretched, as shown in Fig. 1(d). The simple facile fabrication approach to develop the neurological electronic skin, which is based on the all-organic synaptic transistor, is described in the following.

Figure 2(a) present the brief fabrication procedures of the all-organic synaptic transistor. The PEDOT:PSS solution was spin-coated onto a glass substrate with a 25 μm thick Kapton film-based stencil mask. The device channel was formed after the stencil mask was peeled off. The APTES treated PDMS substrate was pressed on the patterned PEDOT:PSS film on the glass and peeled off. By adding the surfactant, the PEDOT nanofibrils (shown in the atomic force microscopy (AFM) image of the prepared PEDOT:PSS film) can form in the PSS/surfactant, which enables this film to be deformable [25]. The P3HT-NFs/PDMS film was formed on the channel region by

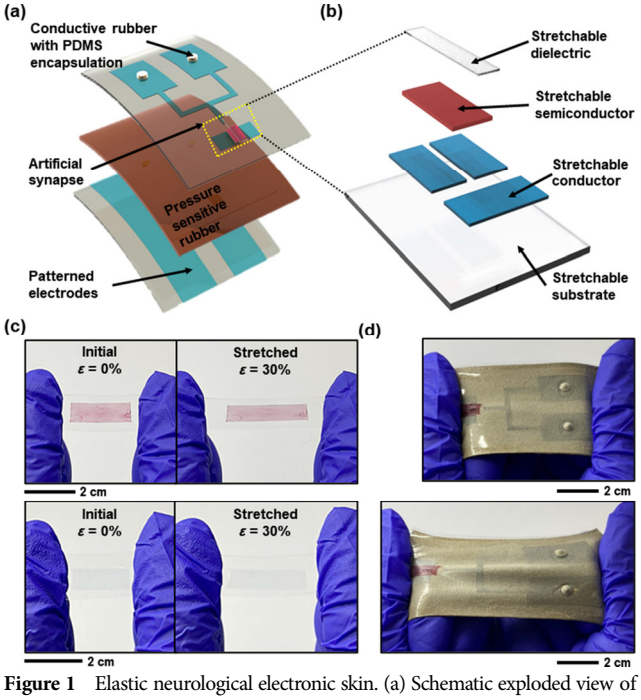

Figure 1 Elastic neurological electronic skin. (a) Schematic exploded view of an elastic neurological electronic skin. (b) Schematic exploded view of a fully rubbery, all-organic synaptic transistor. (c) Optical images of P3HT-NFs/PDMS semiconductor and PEDOT:PSS conductor film on PDMS without and with 30% strain. (d) Optical images of an elastic neurological electronic skin without and with 30% strain.

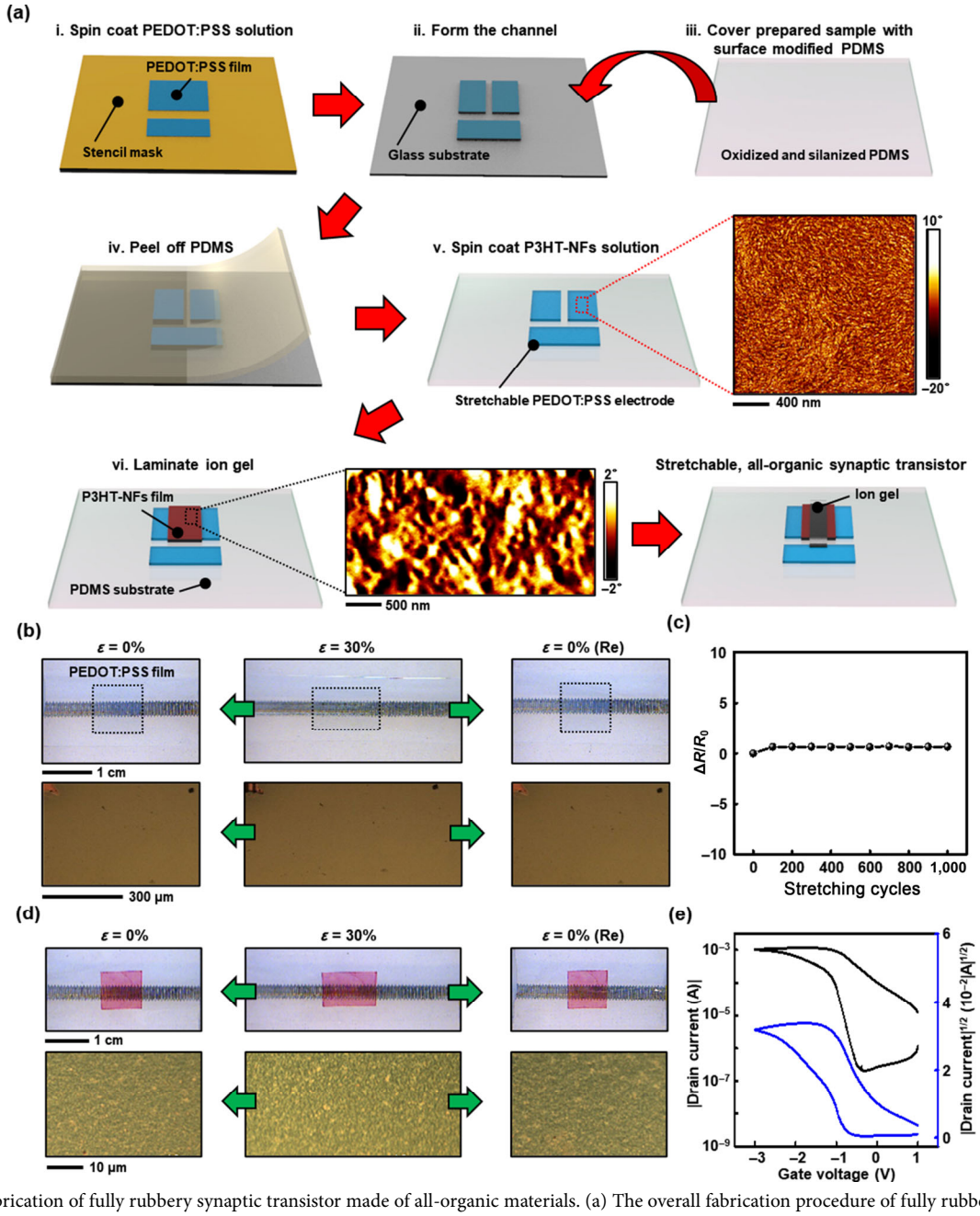

Figure 2 Fabrication of fully rubbery synaptic transistor made of all-organic materials. (a) The overall fabrication procedure of fully rubbery, all-organic synaptic transistor. (b) A set of optical images and microscope images of stretchable PEDOT:PSS film upon stretching by 0, 30, and 0% (released), respectively. (c) Normalized resistance change of PEDOT:PSS film under mechanical strain of 30% depending on the number of stretching cycles. (d) A set of optical images and microscope images of stretchable P3HT-NFs film upon stretching by 0%, 30%, and 0% (released), respectively. (e) Dual sweep transfer curve of fully rubbery, all-organic synaptic transistor.

spin-coating with the Kapton film-based stencil mask. The AFM image of the prepared P3HT-NFs film shows formation of the percolated P3HT-NFs in a rubber matrix, which maintains semiconductor characteristics under mechanical strain [26]. The AFM image of the stretched P3HT-NFs/PDMS film is shown in Fig. S1 in the Electronic Supplementary Material (ESM). The ion-gel was laminated on the P3HT-NFs film to finalize an all-organic synaptic transistor. The detailed experimental conditions are presented in the Experimental section. Figure 2(b) shows a set of optical images and microscope images of the stretchable PEDOT:PSS film upon stretching by 0%, 30%, and 0% (released), respectively. The crack on-set strain is about 45%, as shown in Fig. S2 in the ESM. Figure 2(c) shows the normalized resistance change of the PEDOT:PSS film under repeated cyclic stretching up to 30% strain. The slight resistance increase saturated within the first 100 cycles under a mechanical strain of 30% and no substantial further resistance increase change was observed within additional 900 cycles. The *I*–*V* curve and normalized resistance change of the PEDOT:PSS film during the first stretch-release cycle is shown in Fig. S3 in the ESM. Figure 2(d) shows a set of optical images and microscope images of stretchable P3HT-NFs film upon stretching by 0%, 30%, and 0% (released), respectively. The film did not show surface morphology changes or any crack after cyclic stretching. The transfer curve of the all-organic synaptic transistor is shown in Fig. 2(e). The synaptic transistor showed hysteresis, which is essential for mimicking the biological synapse [3, 27].

Figure 3(a) shows sequential optical images of the all-organic synaptic transistor under mechanical strains of 0%, 10% 20%, 30%, and 0% (released) along the channel length direction. The channel length and width are 100 μm and 5 mm,

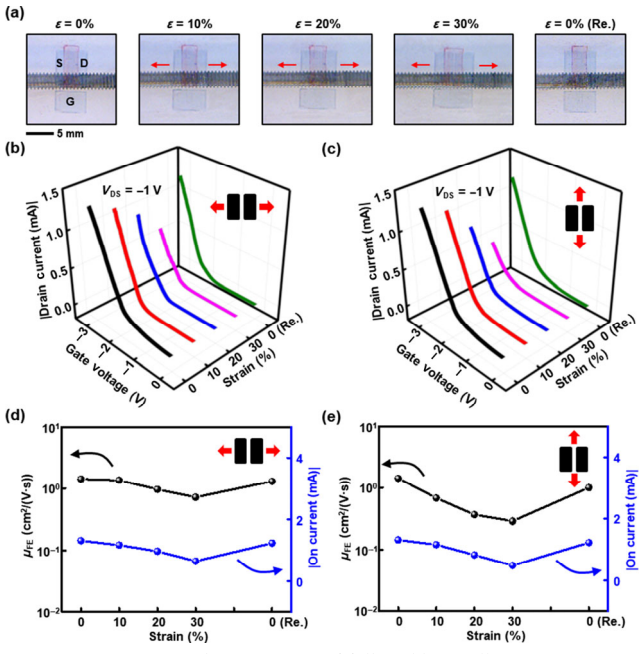

Figure 3 Transistor characteristics of fully rubbery, all-organic synaptic transistor under mechanical strains. (a) Sequential optical images of fully rubbery synaptic transistor made out of all-organic materials under mechanical strains of 0%, 10%, 20%, 30%, and 0% (released) along to the channel length direction. (b) and (c) Transfer curve of fully rubbery, all-organic synaptic transistor under mechanical strains of 0%, 10%, 20%, 30%, and 0% (released) along and perpendicular to the channel length directions, respectively. (d) and (e) On current and μ_{FE} of fully rubbery, all-organic synaptic transistor under mechanical strains of 0%, 10%, 20%, 30%, and 0% (released) along and perpendicular to the channel length directions, respectively.

respectively. The thickness of the P3HT-NFs/PDMS film is ~ 300 nm. Figures 3(b) and 3(c) shows transfer curves of the all-organic synaptic transistor under different levels of mechanical strains along and perpendicular to the channel length directions, respectively. The drain current was obtained while the gate voltage was swept from 0 to –3 V at a drain voltage of –1 V. The maximum drain current of the unstretched synaptic transistor is 1.31 mA. Upon stretching by 10%, 20%, and 30% along the channel length direction, the current decreased to 1.17, 0.74, and 0.65 mA, respectively. Upon fully releasing the mechanical stretching, the current recovered to 1.24 mA. Similar results were observed when the device was stretched and released perpendicular to the channel length direction. We measured and calculated the on current and mobility (μ_{FE}) of the all-organic synaptic transistor under different levels of mechanical strain in Figs. 3(d) and 3(e), respectively.

Figure 4(a) shows a schematic illustration of the synapse and its signal transmission process in the biological nervous system. In synaptic transmission, the nerve impulses (presynaptic signal) from stimulations are generated in the pre-synapse, and then, ion channels of the post-synapse start to open, which induces a change in the electrical signal (postsynaptic signal) of the post-synaptic membrane [28]. Figure 4(b) shows the all-organic synaptic transistor with the ion-gel gate dielectric that emulates biological synaptic functions. In our synaptic transistor, the ions from the ion gel and channel conductance emulate biological neurotransmitters and the synaptic weight, respectively.

To characterize single pulse-induced EPSC, a presynaptic pulse (–3 V) was applied to the gate with a V_{ds} of –1 V with different pulse widths ranging from 50 to 1,000 ms. Figure 4(c) presents the EPSC results of the fully rubbery, all-organic synaptic transistor. It shows that the EPSC increased from 12 to 167 μA

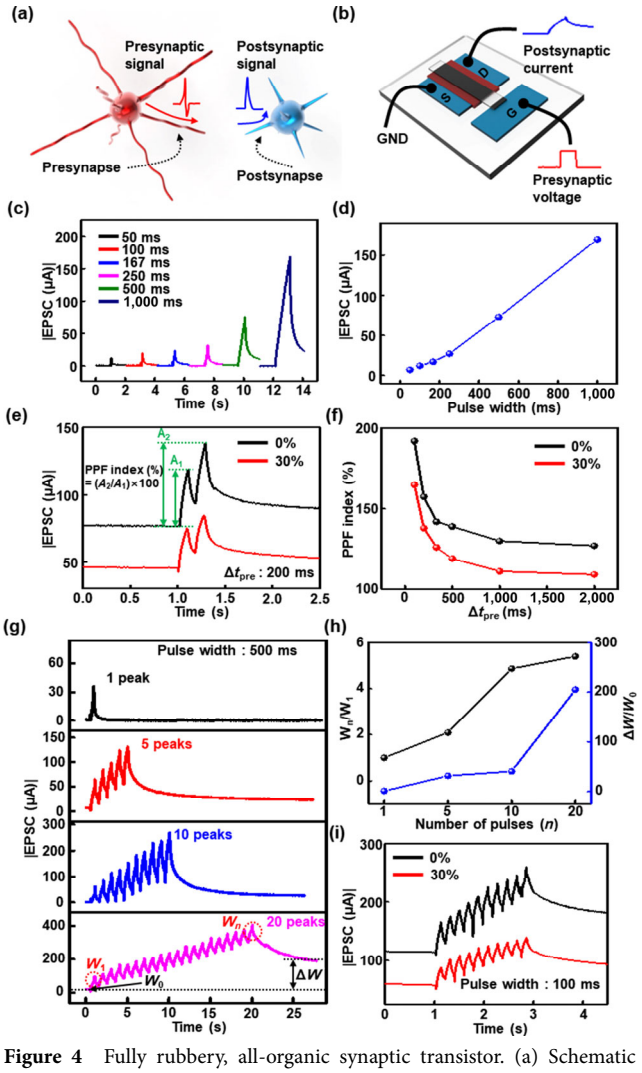

Figure 4 Fully rubbery, all-organic synaptic transistor. (a) Schematic illustration of the synapse and its signal transmission process in the biological nervous system. (b) All-organic synaptic transistor with ion-gel gate dielectric that emulates biological synaptic functions. (c) Single presynaptic pulse induced EPSC with different pulse widths ranging from 50 to 1,000 ms. (d) The EPSC peaks depending on different pulse widths. (e) The EPSC results triggered by two successive presynaptic pulses with Δt_{pre} of 200 ms without and with 30% strain. (f) The PPF index with different Δt_{pre} without and with 30% strain. (g) Memory characteristics of the all-organic synaptic transistor under different number of presynaptic pulses ranging from 1 to 20. (h) W_1/W_n and $\Delta W/W_0$ results of the fully rubbery, all-organic synaptic transistor under different number of presynaptic pulses ranging from 1 to 20. (i) Memory characteristic of fully rubbery, all-organic synaptic transistor without and with 30% strain with the application of the 10 successive presynaptic pulses with a pulse width of 100 ms, a pulse frequency of 5 Hz, and an amplitude of –3 V.

when the pulse width increased from 50 to 1,000 ms. This behavior is due to the increase in ion density at the interface between the ion gel and channel layer, as the pulse width increased [28, 29]. The EPSC peaks depending on different pulse widths are summarized in Fig. 4(d). The EPSC increased when the pulse intensity increased from 3 to 6 V, which can also be attributed to the aforementioned reasoning (Fig. S4 in the ESM).

We further tested the EPSC upon applying two successive presynaptic pulses with pulse intervals (Δt_{pre}) ranging from 100 to 2,000 ms. Figure 4(e) shows the EPSC results triggered by two successive presynaptic pulses with a Δt_{pre} of 200 ms. The EPSC peak from the second pulse (A_2) is greater than that from the first presynaptic pulse (A_1) because part of the induced ions in the first pulse still exist at the interface

between ion gel and channel layer, which results in a higher conductance in the second pulse [30, 31]. The PPF index is defined as $A_2/A_1 \times 100\%$, which can be weakened or strengthened by adjusting the intervals between two successive pulses. The PPF index of 158% was obtained under 0% strain. With 30% applied strain, the PPF index is decreased to 138% because synaptic decay constants decreased with an increase of mechanical strain [32]. The PPF index using different Δt_{pre} without and with 30% strain is plotted in Fig. 4(f). A maximum PPF index of 192% was obtained with a Δt_{pre} of 100 ms under 0% strain and the PPF index decreased when the Δt_{pre} increased from 100 to 2,000 ms. The lower PPF from the long Δt_{pre} is due to the relaxation of the ions [33, 34]. Upon stretching by 30%, the PPF index was still retained.

Memory behaviors such as sensory memory (SM), short-term memory (STM), and long-term memory (LTM), which exist in biological synapses [35], were also characterized. A presynaptic pulse (–3 V) was applied to the gate with a V_{ds} of –1 V with a pulse width of 500 ms. The EPSC peak and memory level increased with the increasing number of presynaptic pulses, as shown in Fig. 4(g). The first and last EPSC peaks are denoted as W_1 and W_n, respectively. The initial current and current change (after the presynaptic pulse) are denoted as W_0 and ΔW, respectively. It is noted that the ΔW was calculated 7 s after the presynaptic pulses were applied. The short-term weight change and long-term weight change are calculated on the basis of W_1/W_n and $\Delta W/W_0$, respectively. Figure 4(h) shows W_1/W_n and $\Delta W/W_0$ results of the fully rubbery, all-organic synaptic transistor. As the number of pulses increases, W_1/W_n increases from 1 to 5.4 and $\Delta W/W_0$ increases from 1.05 to 205. Figure 4(i) shows the EPSC results of the all-organic synaptic transistor without and with 30% strain with the application of the 10 successive presynaptic pulses with a pulse width of 100 ms, a pulse frequency of 5 Hz, and an amplitude of –3 V. With 30% applied strain, the overall EPSC decreased, the W_1/W_n decreased from 1.62 (0% strain) to 1.59 (30% strain), and the $\Delta W/W_0$ decreased from 0.67 (0% strain) to 0.59 (30% strain). These results show that our device still retains memory behaviors even at 30% strain.

We demonstrate the use of our fully rubbery, all-organic synaptic transistor for an elastic neurological electronic skin to illustrate a potential application in HRI. Figure 5(a) shows an optical image of the deformable neurological electronic skin for this HRI system on the

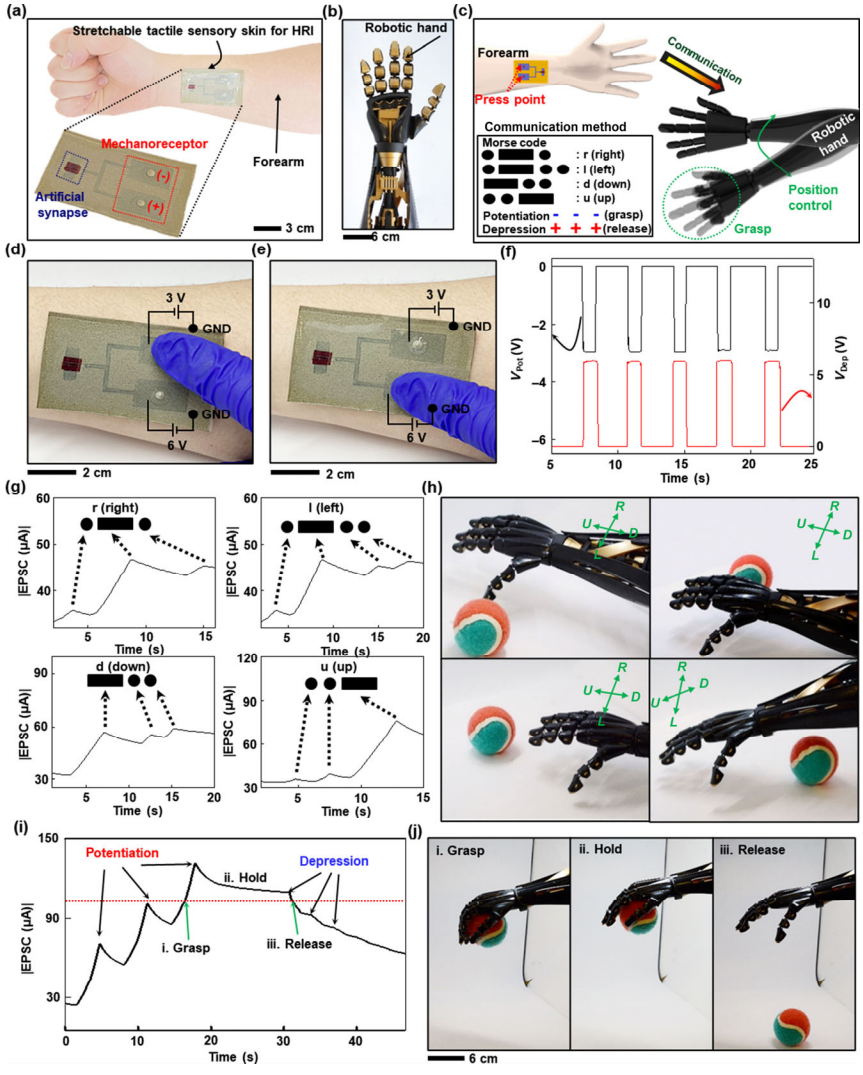

Figure 5 Elastic neurological electronic skin for HRIs. (a) The optical image of an elastic neurological electronics skin for HRI on the forearm. (b) The optical image of robotic hand. (c) Schematic illustration of the HRI system between the robotic hand and the neurological electronic skin. (d) and (e) The optical image of physical touch on the mechanoreceptor for generating presynaptic pulse for both synaptic potentiation and depression, respectively. (f) Presynaptic pulses for synaptic potentiation and depression, generated from mechanoreceptor. (g) The EPSC results decoded by the Morse Code of r (right), l (left), d (down) and u (up) from the neurological electronic skin. (h) The optical images of the motion of the robotic hand depending on the Morse Code decoded signals. (i) The EPSC result during operation of robotic hand such as grasp, hold, and release the object for 46 s. (j) A sequence of images of robotic operation based on the synaptic currents obtained from fully rubbery, all-organic synaptic transistor.

forearm. The electronic skin conformally adhered to the human skin because it is fully made from rubbery materials. The neurological electronic skin consists of the artificial synapse and the mechanoreceptors. Both the artificial synapse and the mechanoreceptors are electrically connected. Figure 5(b) presents a robotic hand (Star Wars Science, Darth Vader robotic arm) which communicates with the neurological electronic skin. The schematic illustration of the HRI system is shown in Fig. 5(c). Action potentials for both synaptic potentiation and depression can be generated by pressing the mechanoreceptor in the electronic skin on the human skin. The action potentials in the form of pulses produced by the mechanoreceptor are transmitted to the artificial synapse, which generates EPSCs. The generated EPSCs are utilized to control the motion of the robotic hand including grasp, release, and move. In particular, different patterns of pressing the mechanoreceptor represent Morse Code, in which the letters of the English alphabet can induce distinct EPSC peaks. Morse Code that is formed by a sequence of dots and dashes, is very secure and thus it was used as communication method for HRIs [36]. Figure 5(d) shows the optical image of pressing the mechanoreceptor that generates negative potentials in the electronic skin (i.e., potentiation of the postsynaptic current). When tapping with applied pressure higher than 100 kPa on pressure-sensitive rubber was performed, presynaptic pulse was obtained. The resistance change depending on applied pressure is presented in Fig. S5 in the ESM. Pressing the mechanoreceptor that generates positive potentials in the electronic skin is presented in Fig. 5(e), which causes depression of the postsynaptic current. The information of both negative and positive potentials is shown in Fig. 5(f). We demonstrated different EPSCs depending on the letter of the English alphabet. The EPSCs decoded by the Morse Code corresponding to the letters 'r', 'l', 'd' and 'u' indicate the movement direction of robotic hand, such as right, left, down and up, respectively, as shown in Fig. 5(g). The four letters were correlated with the sum of the amplitude of the EPSC peaks (Fig. S6 in the ESM). The frequency of the presynaptic voltage for the symbol of the circle and rectangle were 0.5 and 0.167 Hz, respectively, which can be controlled by changing the time of pressing the mechanoreceptor. Figure 5(h) shows images of the motion of the robotic hand depending on the Morse Code decoded signals, respectively. The robotic hand moves depending on the created EPSC behaviors from the electronic skin to approach the targeted object. Figure 5(i) presents the EPSC results during operation of the robotic hand such as grasp, hold, and release the object for 46 s. The three successive potentiation pulses result in an EPSC that is higher than the threshold point (100 μA), which causes the robotic hand to grasp the object. After applying the potentiation pulses, no additional pulses were applied, and thus the EPSC slowly decreased for 9 s (rest). The depression pulses make the EPSC lower than the threshold point, which allows the robotic hand to release the object. Figure 5(j) shows a sequence of images of robotic operation based on the synaptic currents obtained from the fully rubbery, all-organic synaptic transistor.

4 Conclusions

We developed a fully rubbery synaptic transistor using all-organic materials for the rubbery substrate, conductor, semiconductor, and dielectric. The synaptic transistor showed unique functions existing in biological synapses, including EPSC, PPF, and memory characteristics. The synaptic transistor retained its functionality while being stretched by 30% both along and perpendicular to the channel length direction. We further developed an elastic neurological electronic skin in a fully rubbery format based on two mechanoreceptors (for synaptic potentiation or depression) consisting of pressure-sensitive rubber and a fully rubbery synaptic transistor. One exemplary usage of the fully rubbery, all-organic synaptic transistor in the elastic neurological electronic skin is to enable HRI. By converting tactile signals into Morse Code, potentiation and depression of EPSC signals, the neurological electronic skin on a human forearm was successfully used as a communication device between the human and robot. Such elastic all-organic synaptic transistor and its integrated neurologic skin pave the way towards low-cost, facile processable, biocompatible, soft, functional biomimetic systems.

Data availability

All data needed to evaluate the conclusions in the paper are present in the paper and/or the Supplementary Materials. Additional data related to this paper may be requested from the authors.

Author contribution

H. S. and C. Y. conceived and designed the experiment. H. S., S. J., K. S., and J. G. J. performed the experiments. H. S., S. J., and Z. R. characterized device performance. H. S. analyzed the experimental data. J. G. J., and J.-I. H., advised on materials characterization. H. S., and C. Y. wrote the paper.

Acknowledgments

C. Y. would like to thank financial support by the Office of Naval Research grant (N00014-18-1-2338) under Young Investigator Program, the National Science Foundation grants of CAREER (1554499), EFRI (1935291), and CPS (1931893).

Electronic Supplementary Material: Supplementary material (detailed characterization of rubbery materials, device characteristics of synaptic transistor and skin devices) is available in the online version of this article at https://doi.org/10.1007/s12274-021-3602-x.

References

[1] Thompson, W. Synapse elimination in neonatal rat muscle is sensitive to pattern of muscle use. *Nature* **1983**, *302*, 614–616.

[2] Chortos, A.; Liu, J.; Bao, Z. N. Pursuing prosthetic electronic skin. *Nat. Mater.* **2016**, *15*, 937–950.

[3] Shim, H.; Sim, K.; Ershad, F.; Yang, P. Y.; Thukral, A.; Rao, Z. Y.; Kim, H. J.; Liu, Y. H.; Wang, X.; Gu, G. Y. et al. Stretchable elastic synaptic transistors for neurologically integrated soft engineering systems. *Sci. Adv.* **2019**, *5*, eaax4961.

[4] Zhu, L. Q.; Wan, C. J.; Guo, L. Q.; Shi, Y.; Wan, Q. Artificial synapse network on inorganic proton conductor for neuromorphic systems. *Nat. Commun.* **2014**, *5*, 3158.

[5] Andreae, L. C.; Burrone, J. The role of spontaneous neurotransmission in synapse and circuit development. *J. Neurosci. Res.* **2018**, *96*, 354–359.

[6] Kim, S.; Lee, B.; Reeder, J. T.; Seo, S. H.; Lee, S. U.; Hourlier-Fargette, A.; Shin, J.; Sekine, Y.; Jeong, H.; Oh, Y. S. et al. Soft, skin-interfaced microfluidic systems with integrated immunoassays, fluorometric sensors, and impedance measurement capabilities. *Proc. Natl. Acad. Sci. USA* **2020**, *117*, 27906–27915.

[7] Rogers, J. A. Nanomesh on-skin electronics. *Nat. Nanotechnol.* **2017**, *12*, 839–840.

[8] Wang, C.; Hwang, D.; Yu, Z. B.; Takei, K.; Park, J.; Chen, T.; Ma, B. W.; Javey, A. User-interactive electronic skin for instantaneous pressure visualization. *Nat. Mater.* **2013**, *12*, 899–904.

[9] Yokota, T.; Zalar, P.; Kaltenbrunner, M.; Jinno, H.; Matsuhisa, N.; Kitanosako, H.; Tachibana, Y.; Yukita, W.; Koizumi, M.; Someya, T. Ultraflexible organic photonic skin. *Sci. Adv.* **2016**, *2*, e1501856.
[10] Kim, Y.; Chortos, A.; Xu, W. T.; Liu, Y. X.; Oh, J. Y.; Son, D.; Kang, J.; Foudeh, A. M.; Zhu, C. X.; Lee, Y. A bioinspired flexible organic artificial afferent nerve. *Science* **2018**, *360*, 998–1003.
[11] Akbari, M. K.; Zhuiykov, S. A bioinspired optoelectronically engineered artificial neurorobotics device with sensorimotor functionalities. *Nat. Commun.* **2019**, *10*, 3873.
[12] Zhang, X. M.; Zhuo, Y.; Luo, Q.; Wu, Z. H.; Midya, R.; Wang, Z. R.; Song, W. H.; Wang, R.; Upadhyay, N. K.; Fang, Y. L. et al. An artificial spiking afferent nerve based on mott memristors for neurorobotics. *Na t. Commun.* **2020**, *11*, 51.
[13] Keene, S. T.; Lubrano, C.; Kazemzadeh, S.; Melianas, A.; Tuchman, Y.; Polino, G.; Scognamiglio, P.; Cinà, L.; Salleo, A.; Van De Burgt, Y. et al. A biohybrid synapse with neurotransmitter-mediated plasticity. *Nat. Mater.* **2020**, *19*, 969–973.
[14] Sim, K.; Rao, Z. Y.; Zou, Z. N.; Ershad, F.; Lei, J. M.; Thukral, A.; Chen, J.; Huang, Q. A.; Xiao, J. L.; Yu, C. J. Metal oxide semiconductor nanomembrane–based soft unnoticeable multifunctional electronics for wearable human-machine interfaces. *Sci. Adv.* **2019**, *5*, eaav9653.
[15] Wan, C. J.; Cai, P. Q.; Wang, M.; Qian, Y.; Huang, W.; Chen, X. D. Artificial sensory memory. *Adv. Mater.* **2020**, *32*, 1902434.
[16] Wan, C. J.; Cai, P. Q.; Guo, X. T.; Wang, M.; Matsuhisa, N.; Yang, L.; Lv, Z. S.; Luo, Y. F.; Loh, X. J.; Chen, X. D. An artificial sensory neuron with visual-haptic fusion. *Nat. Commun.* **2020**, *11*, 4602.
[17] Wan, H. C.; Cao, Y. Q.; Lo, L. W.; Zhao, J. Y.; Sepúlveda, N.; Wang, C. Flexible carbon nanotube synaptic transistor for neurological electronic skin applications. *ACS Nano* **2020**, *14*, 10402–10412.
[18] Zang, Y. P.; Shen, H. G.; Huang, D. Z.; Di, C. A.; Zhu, D. B. A dual-organic-transistor-based tactile-perception system with signal-processing functionality. *Adv. Mater.* **2017**, *29*, 1606088.
[19] Forrest, S. R. The path to ubiquitous and low-cost organic electronic appliances on plastic. *Nature* **2004**, *428*, 911–918.
[20] Ruiz, C.; García-Frutos, E. M.; Hennrich, G.; Gómez-Lor, B. Organic semiconductors toward electronic devices: High mobility and easy processability. *J. Phys. Chem. Lett.* **2012**, *3*, 1428–1436.
[21] Someya, T.; Bao, Z. N.; Malliaras, G. G. The rise of plastic bioelectronics. *Nature* **2016**, *540*, 379–385.
[22] Lanzani, G. Organic electronics meets biology. *Nat. Mater.* **2014**, *13*, 775–776.
[23] Sekitani, T.; Someya, T. Stretchable, large-area organic electronics. *Adv. Mater.* **2010**, *22*, 2228–2246.
[24] Lipomi, D. J.; Bao, Z. N. Stretchable and ultraflexible organic electronics. *MRS Bull.* **2017**, *42*, 93–97.
[25] Oh, J. Y.; Kim, S.; Baik, H. K.; Jeong, U. Conducting polymer dough for deformable electronics. *Adv. Mater.* **2016**, *28*, 4455–4461.
[26] Kim, H. J.; Sim, K.; Thukral, A.; Yu, C. J. Rubbery electronics and sensors from intrinsically stretchable elastomeric composites of semiconductors and conductors. *Sci. Adv.* **2017**, *3*, e1701114.
[27] Molina-Lopez, F.; Gao, T. Z.; Kraft, U.; Zhu, C.; Öhlund, T.; Pfattner, R.; Feig, V. R.; Kim, Y.; Wang, S.; Yun, Y. et al. Inkjet-printed stretchable and low voltage synaptic transistor array. *Nat. Commun.* **2019**, *10*, 2676.
[28] Yang, Q.; Yang, H. H.; Lv, D. X.; Yu, R. J.; Li, E. L.; He, L. H.; Chen, Q. Z.; Chen, H. P.; Guo, T. L. High-performance organic synaptic transistors with an ultrathin active layer for neuromorphic computing. *ACS Appl. Mater. Interfaces* **2021**, *13*, 8672–8681.
[29] Gao, W. T.; Zhu, L. Q.; Tao, J.; Wan, D. Y.; Xiao, H.; Yu, F. Dendrite integration mimicked on starch-based electrolyte-gated oxide dendrite transistors. *ACS Appl. Mater. Interfaces* **2018**, *10*, 40008–40013.
[30] Yu, J. R.; Gao, G. Y.; Huang, J. R.; Yang, X. X.; Han, J.; Zhang, H.; Chen, Y. H.; Zhao, C. L.; Sun, Q. J.; Wang, Z. L. Contact-electrification-activated artificial afferents at femtojoule energy. *Nat. Commun.* **2021**, *12*, 1581.
[31] Wei, H. H.; Shi, R. C.; Sun, L.; Yu, H. Y.; Gong, J. D.; Liu, C.; Xu, Z. P.; Ni, Y.; Xu, J. L.; Xu, W. T. Mimicking efferent nerves using a graphdiyne-based artificial synapse with multiple ion diffusion dynamics. *Nat. Commun.* **2021**, *12*, 1068.
[32] Wang, X. M.; Yan, Y. J.; Li, E. L.; Liu, Y. Q.; Lai, D. X.; Lin, Z. X.; Liu, Y.; Chen, H. P.; Guo, T. L. Stretchable synaptic transistors with tunable synaptic behavior. *Nano Energy* **2020**, *75*, 104952.
[33] Yu, F.; Zhu, L. Q.; Gao, W. T.; Fu, Y. M.; Xiao, H.; Tao, J.; Zhou, J. M. Chitosan-based polysaccharide-gated flexible indium tin oxide synaptic transistor with learning abilities. *ACS Appl. Mater. Interfaces* **2018**, *10*, 16881–16886.
[34] Zhu, J. D.; Yang, Y. C.; Jia, R. D.; Liang, Z. X.; Zhu, W.; Rehman, Z. U.; Bao, L.; Zhang, X. X.; Cai, Y. M.; Song, L. et al. Ion gated synaptic transistors based on 2d van der Waals crystals with tunable diffusive dynamics. *Adv. Mater.* **2018**, *30*, 1800195.
[35] Ohno, T.; Hasegawa, T.; Tsuruoka, T.; Terabe, K.; Gimzewski, J. K.; Aono, M. Short-term plasticity and long-term potentiation mimicked in single inorganic synapses. *Nat. Mater.* **2011**, *10*, 591–595.
[36] Gu, J. H.; Park, M.; Kang, K.; Shin, H. C. Morse code representation using emg signals. In *2019 International Conference on Information and Communication Technology Convergence (ICTC)*, Jeju, Korea, 2019, pp 1059–1061.